Available online at www.sciencedirect.com

ScienceDirect

J Materiomics 2 (2016) 141–149

www.ceramsoc.com/en/

www.journals.elsevier.com/journal-of-materiomics/

Enhanced thermoelectric performance of PbTe bulk materials with figure of merit zT >2 by multi-functional alloying

Tiezheng Fu [a], Xianqiang Yue [a], Haijun Wu [b], Chenguang Fu [a], Tiejun Zhu [a,*], Xiaohua Liu [a], Lipeng Hu [a], Pingjun Ying [a], Jiaqing He [b], Xinbing Zhao [a,**]

[a] State Key Laboratory of Silicon Materials, School of Materials Science and Engineering, Zhejiang University, Hangzhou 310027, China
[b] Department of Physics, South University of Science and Technology of China, Shenzhen 518055, China

Received 29 March 2016; revised 5 May 2016; accepted 7 May 2016
Available online 13 May 2016

Abstract

Forming solid solutions in PbTe based materials can simultaneously reduce lattice thermal conductivity and engineer the band structure to enhance the electrical properties. In this paper, quaternary alloys of $Pb_{1-x}Mg_xTe_{0.8}Se_{0.2}$ were designed to improve the figure of merit zT. The significant roles of MgTe in enhancing electrical properties and reducing thermal conductivity of $PbTe_{0.8}Se_{0.2}$ were investigated. A maximum zT of ~2.2 at 820 K was achieved in $PbTe_{0.8}Se_{0.2}$ with 8% MgTe. Subsequently, a large dimension bulk (~200 g, Φ42 mm × 18 mm) was fabricated and its homogeneity and the repeatability of high zT values were determined. The results show that high zT ~2.0 can also be achieved even in such a large sample. These results highlight the multi-functional roles of quaternary alloying with Mg and Se, and demonstrate the realistic prospect of large-scale commercial fabrication in high performance PbTe-based thermoelectric materials.

Keywords: Thermoelectric; Alloying; PbTe; Band engineering; Thermal conductivity

1. Introduction

The increasing demand for sustainable energy conversion technologies has attracted worldwide interest in thermoelectric (TE) materials, which can directly convert waste heat into electricity [1,2]. The conversion efficiency of TE devices is represented by the materials' dimensionless figure of merit $zT = \alpha^2\sigma T/(\kappa_e + \kappa_L)$, where α is the Seebeck coefficient, σ is the electrical conductivity, T is the absolute temperature, κ_e and κ_L are the electrical and lattice contribution to the total thermal conductivity κ, respectively [1,3,4].

Given the less inter-dependence between the electrical properties and the lattice thermal conductivity, two basic strategies are widely used to improve the TE performance. One is to enhance the electrical power factor ($PF = \alpha^2\sigma$) through band engineering such as converging the electronic bands or introducing the resonant levels, *etc*. [5–9]. The other is to reduce the lattice thermal conductivity κ_L by introducing multiscale phonon scattering centers, *i.e.* point defects, grain boundaries, nano-precipitates, *etc*. [10–13].

PbTe-based alloys are one of the most promising TE materials for power generation in intermediate temperature range (600–800 K) [14]. Historically, PbTe was used to provide power for space crafts [15]. In recent decades, a great progress has been made to get higher zTs in PbTe-based materials. A zT of ~2.2 at 915 K was obtained in p-type PbTe–SrTe (4 mol%) doped with 2 mol% Na [11]. It was proven that forming solid solutions is one of the most effective and practical ways to improve zT values in some TE materials such as $Mg_2Si_{1-z}Sn_z$ [16,17], $Sn_{1-x}Mn_xTe$ [6,18,19], and PbTe based materials [5,10,20–22]. When solid solutions are formed, two significant effects can be expected, *i.e.*reducing

* Corresponding author.
** Corresponding author.
E-mail addresses: zhutj@zju.edu.cn (T. Zhu), zhaoxb@zju.edu.cn (X. Zhao).
Peer review under responsibility of The Chinese Ceramic Society.

http://dx.doi.org/10.1016/j.jmat.2016.05.005

lattice thermal conductivity and optimizing the electrical properties. The atomic disorders induced from point defects produce the mass and size fluctuations in crystals, which can effectively scatter the high-frequency phonons. Forming solid solutions can also engineer the band structures, such as in p-type $PbTe_{1-x}Se_x$ [5] systems and $Mg_xPb_{1-x}Te$ [10,22] systems. For example, a zT of 1.6 was obtained in $Pb_{0.98}Tl_{0.02}Te_{1-x}S_x$ solid solutions as $x = 0.08$ by a combination of alloy phonon scattering and resonant electronic levels [8]. In the case of p-type $PbTe_{1-x}Se_x$ systems, a maximum zT of 1.8 was achieved due to the increased valley degeneracy and reduced lattice thermal conductivity [5]. However, little work have been reported on the quaternary alloying of $PbTe_{1-x}Se_x$ systems. In $Mg_xPb_{1-x}Te$ system, Mg alloying can modify the structure of valence bands, resulting in a less-temperature-dependent optimal carrier concentration [22]. Once the content of Mg exceeds its solubility limit in PbTe matrix (~6% for $T > 525$ K), nanophases would precipitate and the lattice thermal conductivity can be further reduced [10]. So a lower lattice thermal conductivity can be expected in properly doped $Mg_xPb_{1-x}Te_{1-y}Se_y$ solid solutions as the result of alloy scattering induced by Mg and Se substitution. At the same time, Mg alloying can further modify the band structures of the $PbTe_{1-y}Se_y$ system to obtain a wider band gap and then suppress the bipolar conduction at high temperatures.

It is noteworthy that most of the high zTs were reported in small size samples, *i.e.* 1–2 g per sample. To develop TE device and then satisfy the commercial demands, large-size samples should be fabricated and the composition homogeneity is also required. Repeatable high zT values measured in various parts of the large sample is an effective criterion to characterize the quality of the large-size samples. And it also can mean the high zT values are reliable and repeatable.

In this work, we prepared $Pb_{1-x}Mg_xTe_{0.8}Se_{0.2}$ solid solutions with the optimized Na doping. The $PbTe_{0.8}Se_{0.2}$ was adopted as the matrix due to a zT of ~1.8 obtained in previous work [5]. The effects of Mg alloying on the TE performance of $PbTe_{0.8}Se_{0.2}$ were systematically investigated. It is found that the power factor is increased by 15% and the lattice thermal conductivity is reduced by 20% at 800 K. A maximum zT of ~2.2 is obtained at 820 K for the sample of $Mg_{0.08}Pb_{0.92}Te_{0.8}Se_{0.2}$ with 2% Na doping. Furthermore, the sample was magnified up to ~200 g in weight. In order to check the repeatability and the composition homogeneity in large-size sample, small platelets (Φ12.7 mm × 2 mm) were cut from different parts of the large bulk and their TE properties were measured. It is shown that the average zTs reach ~2.0.

2. Experimental procedure

Samples of $Pb_{1-x}Mg_xTe_{0.8}Se_{0.2}$ ($x = 0$, 0.01, 0.02, 0.03, 0.04, 0.06 and 0.08) were synthesized with 2% sodium as p-type dopant. Appropriate ratios of high pure raw materials (lead 99.99%, tellurium 99.999%, selenium 99.999%, sodium 99.98% and magnesium 99.98%) were loaded into carbon coated quartz tubes in a glove box filled with Ar. The tubes were sealed with high vacuum ~10^{-4} Torr, then heated to 1273 K and melt for 10 h in furnace. The ingots obtained by air quenching were annealed at 873 K for 4 days to ensure the compositional homogeneity. Then the ingots were ground into fine powders. The obtained powders were loaded into the graphite die (Φ12.7 mm for small samples and Φ42 mm for large-size sample) and compacted by spark plasma sintering (SPS) in vacuum at 823 K under 60 MPa. The obtained samples were about 2 g with a dimension of Φ12.7 mm × 2 mm and 200 g with a dimension of Φ42 mm × 18 mm. All pellets have a similar packing density (>95%).

The phase structures of samples were determined by X-ray diffraction (XRD) on a Rigaku D/MAX02550PC X-Ray diffractometer with monochromatic Cu K_α radiation. The obtained samples were cut and polished for electrical and thermal property measurements. The thermal conductivity measurement was measured by a laser flash method (LFA457, Netzsch). The total thermal conductivity was calculated by the equation $\kappa_{tot} = \rho\lambda C_p$, where ρ is density calculated by the dimensions and mass of samples, λ is thermal diffusivity measured by LFA 457, and C_p is specific heat estimated from the relation C_p ($Jg^{-1}K^{-1}$) $= (3.91 \times 10^{-3} \times T + 24.35) \times N_a/M$, where T is the Kelvin temperature, N_a is the atom number in a molecule and M is relative molecular mass [23,24]. The electrical conductivity and Seebeck coefficient were measured using a DC four-probe method and differential voltage/temperature technique, respectively [25]. The Hall measurement at room temperature was measured using a Mini Cryogen Free measurement system. The magnetic field varies from 4 T to −4 T with a step of 0.5 T. The Hall carrier concentration (p_H) and the carrier mobility (μ_H) were estimated by the relation $p_H = 1/eR_H$ and $\mu_H = \sigma R_H$, where e is the carrier charge and R_H is Hall coefficient.

3. Results and discussion

3.1. Electrical transport properties

Fig. 1 presents the XRD patterns of $Pb_{1-x}Mg_xTe_{0.8}Se_{0.2}$ ($x = 0$–0.08) samples. All samples show a typical NaCl-type face centered cubic (FCC) structure. No trace of Na_2Te or MgTe phase, the common secondary phase in PbTe, appears within the detection limit of XRD. All the peaks locate between the diffraction peaks of PbTe (JCPDS#77-0246) and PbSe (JCPDS#89-7105), indicating the formation of the solid solution.

Fig. 2 shows the electrical transport properties for $Pb_{1-x}Mg_xTe_{0.8}Se_{0.2}$ samples with 2% Na doping as a function of temperature. The electrical conductivity decreases with increasing temperature, showing a typical conduction behavior of heavily doped degenerate semiconductor.

The carrier concentration of $Pb_{1-x}Mg_xTe_{0.8}Se_{0.2}$ doped with 2% Na ranges from 9×10^{19} cm^{-3} to 1.2×10^{20} cm^{-3} (Table 1), which is in good agreement with the previous work, such as 2.5×10^{20} cm^{-3} of $PbTe_{1-x}Se_x$ with 2% Na doped [5], and 7.8×10^{19} cm^{-3} of $Mg_{0.03}Pb_{0.97}Te$ with 2% Na doped [22]. Alloying with Mg affects the electrical conductivity as the carrier concentration and carrier mobility are related to the Mg content in matrix $PbTe_{0.8}Se_{0.2}$. The competition between Mg and Na to substitute Pb sites leads to a slight deviation

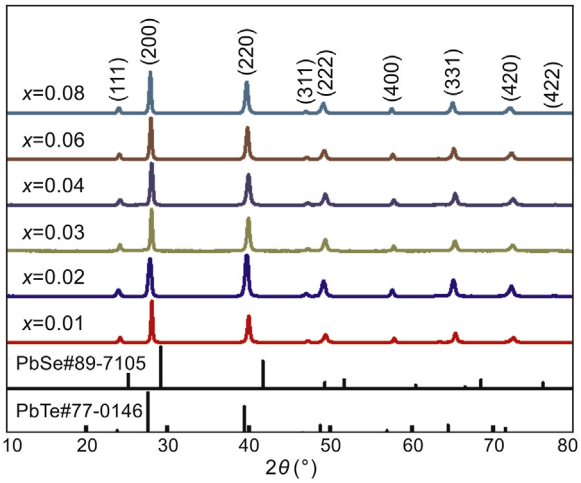

Fig. 1. XRD patterns for $Pb_{1-x}Mg_xTe_{0.8}Se_{0.2}$ ($x = 0$–0.08) samples.

from the nominal doping level. At room temperature, a high electrical conductivity of ~1.88×10^5 S m^{-1} for the Mg-free sample is obtained, which reduces to ~2.7×10^4 S m^{-1} at 820 K. In Fig. 2(a), the electrical conductivities of PbTe (p_H–7.5×10^{19} cm^{-3}) [26] and $Pb_{0.94}Mg_{0.06}Te$ (p_H–8.7×10^{19} cm^{-3}) [10] are plotted for comparison. The electrical conductivity of the quaternary alloying system is lower than that of PbTe in the whole temperature range, because the carrier mobility of solid solutions is much lower than that in the PbTe compound due to the alloy scattering on the carriers. Alloy scattering greatly reduce the mobility at room temperature and the scattering effect decreases with the increase of temperature. It can be found that the electrical conductivity of all the samples tends to be close at high temperatures (700–800 K). The temperature dependence of mobility relies on both scattering mechanism and the effective mass m^*. In p-type PbTe-based materials, m^* increases with temperature, resulting from the band convergence [5,27,28]. Therefore, at high temperature a faster decrease of electrical conductivity with temperature can be expected. Fig. 2(b) is the plot of $\lg\sigma$–$1/T$ and two slopes in the curves of the electrical conductivity against temperature can be observed, where a faster reduction at higher temperatures is shown by larger slope due to the effect of the band convergence and the possible intervalley scattering.

The positive Seebeck coefficient of all samples indicates the p-type conduction due to the sodium doping, shown in Fig. 2(c). The peak value of Seebeck coefficient can be viewed as a sign of bipolar conduction. Since there are opposite effects on the Seebeck coefficient from electrons (minority carriers) and holes (majority carriers), suppressing the bipolar excitation is a key issue to improving zT at high temperatures. The common solution is to either increase majority carrier concentration or widen the band gap at high temperatures.

For $PbTe_{1-x}Se_x$ systems, the band gap between the L band at low temperature (Σ band at high temperature) and the conduction band (C band) is both temperature and composition dependent. Substitution of Se for Te can increase the energy of L band while reduce the energy of Σ band, resulting

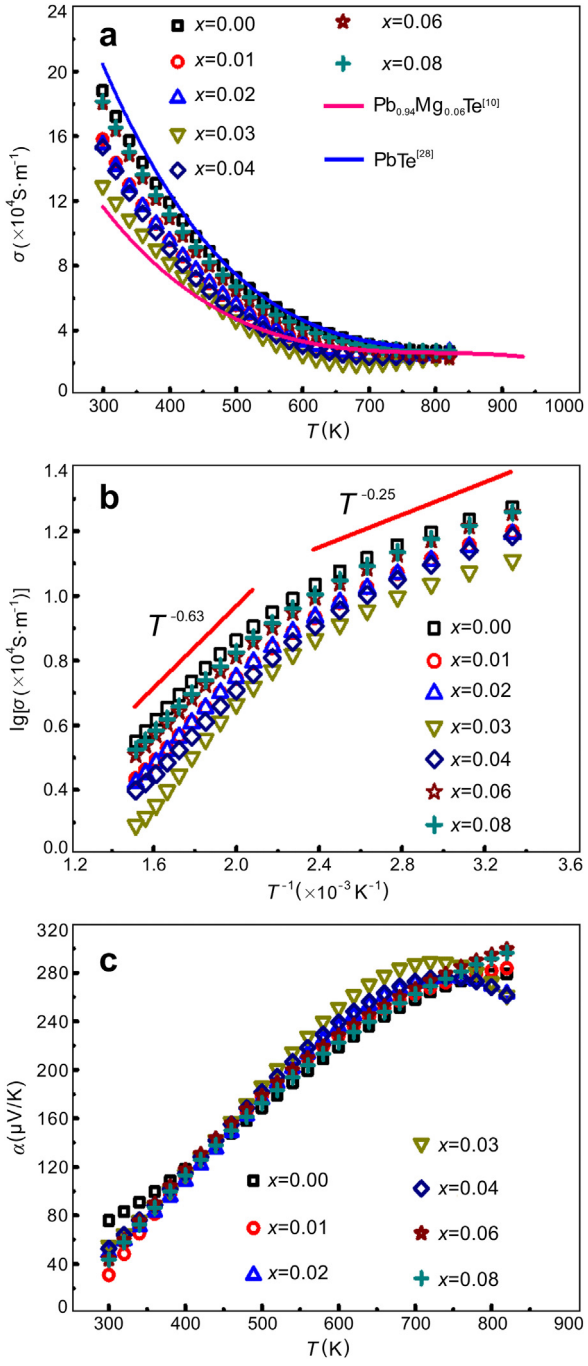

Fig. 2. Temperature dependences of electrical conductivity (a) (b) and Seebeck coefficient (c) for all $Pb_{1-x}Mg_xTe_{0.8}Se_{0.2}$ samples with 2% Na doped. In Fig. 2(a), the solid lines are the electrical conductivities of PbTe (Ref. [28]) and $Pb_{0.94}Mg_{0.06}Te$ (Ref. [10]). Fig. 2(b) is the plot of $\lg\sigma$–$1/T$, indicating two slopes in the variation of the electrical conductivity against temperature.

in a wider band offset between heavy hole band and conduction band $E_{C\text{-}\Sigma}$ at high temperatures, when the L band is lower than the Σ band. The widened band gap is expected to effectively suppress the bipolar diffusion [5]. This effect can be enhanced by further alloying with Mg as MgTe has a larger band gap (~3.5 eV at 300 K) [29]. However, Mg and Se have opposite effects on the band offset between the light valence band and the conduction band $\Delta E_{C\text{-}L}$ as Mg can

Table 1
Thermoelectric properties of $Pb_{1-x}Mg_xTe_{0.8}Se_{0.2}$ doped with 2% Na at 300 K.

Samples	p_H (10^{20} cm^{-3})	μ_H (cm^{2}V^{-1} s^{-1})	zT_{max}
$x = 0$	1.1	106.8	1.8
$x = 0.01$	1.2	82.3	2.0
$x = 0.02$	1.1	88.1	2.0
$x = 0.03$	1.0	83.1	1.9
$x = 0.04$	0.9	103.9	1.8
$x = 0.06$	0.9	129.3	2.1
$x = 0.08$	1.2	94.3	2.2

widen the band gap while Se substitution narrows the band gap around room temperature. As a result, the $PbTe_{0.8}Se_{0.2}$ samples alloyed with Mg will have a smaller band offset between the two valence bands $\Delta E_{L\text{-}\Sigma}$, which is illustrated clearly in Fig. 3. It means the heavy valence band will contribute more to transport properties at low temperature. Thus, a faster increase of the Seebeck coefficient (a larger slope) at low temperatures (300–550 K) can be observed for the Mg alloying samples than the Mg-free sample, as shown in Fig. 2(c). Benefiting from multi-alloying with Mg and Se, the Seebeck coefficient reaches ~300 μV K^{-1} for the samples $x = 0.06$ and $x = 0.08$ at 820 K, showing no sign of bipolar diffusion as a result of the widened band gap $\Delta E_{C\text{-}\Sigma}$.

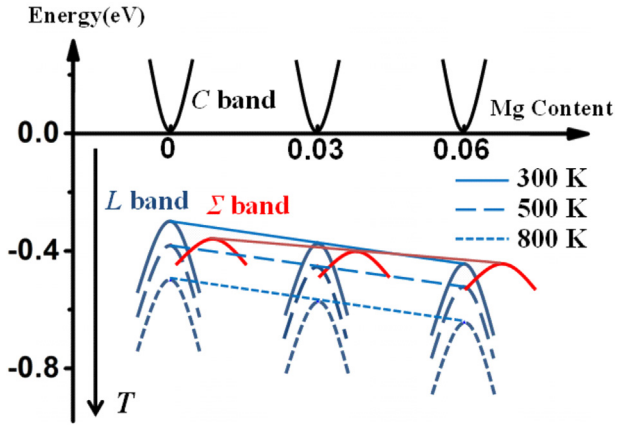

Fig. 3. Schematic band structures for PbTe with Mg alloyed at different temperatures.

Alloying with Mg is more helpful than alloying with Se in maintaining a wider band gap as MgTe has a larger band gap than PbSe. However, the solubility limit of MgTe in PbTe matrix is quite small (~6% for $T > 525$ K) [22,30]. In this case, the solubility can be enhanced in Mg alloyed $PbTe_{1-y}Se_y$ system, which can be confirmed by the electrical property difference between $x = 0.06$ and $x = 0.08$ samples.

3.2. Thermal transport properties

The temperature dependence of total and lattice thermal conductivity is shown in Fig. 4. The decrease in thermal conductivity with increasing temperature is expected for heavily doped semiconductors due to the phonon–phonon Umklapp scattering. The lattice thermal conductivity was calculated by subtracting the electronic contribution from the total thermal conductivity $\kappa_L = \kappa_{tot} - \kappa_e$. According to the Wiedemann-Franz Law, the κ_e is proportional to the electrical conductivity, $\kappa_e = L\sigma T$. Lorenz number L was calculated using the single parabolic band (SPB) model, which results in a difference less than 10% compared with a rigorous single non-parabolic band model or multiple band model calculation [31].The calculated L values decrease with increasing temperature for all the samples. The room temperature L values vary from 2.05 to 2.35 × 10^{-8} WΩK^{-2}.

Alloying with Mg or Se can reduce the lattice thermal conductivity of PbTe, as shown in Fig. 4(b). The room temperature κ_L is significantly reduced from ~2.85 Wm^{-1} K^{-1} for PbTe to ~1.78 Wm^{-1} K^{-1} for $Pb_{0.94}Mg_{0.06}Te$ and ~1.42 Wm^{-1} K^{-1} for $PbTe_{0.8}Se_{0.2}$ ($x = 0$). Multiple alloying with Mg and Se can strengthen the effect of alloy scattering in reducing the κ_L as the atomic disorders induced from point defects can strongly scatter the high frequency phonons. The room temperature κ_L can be

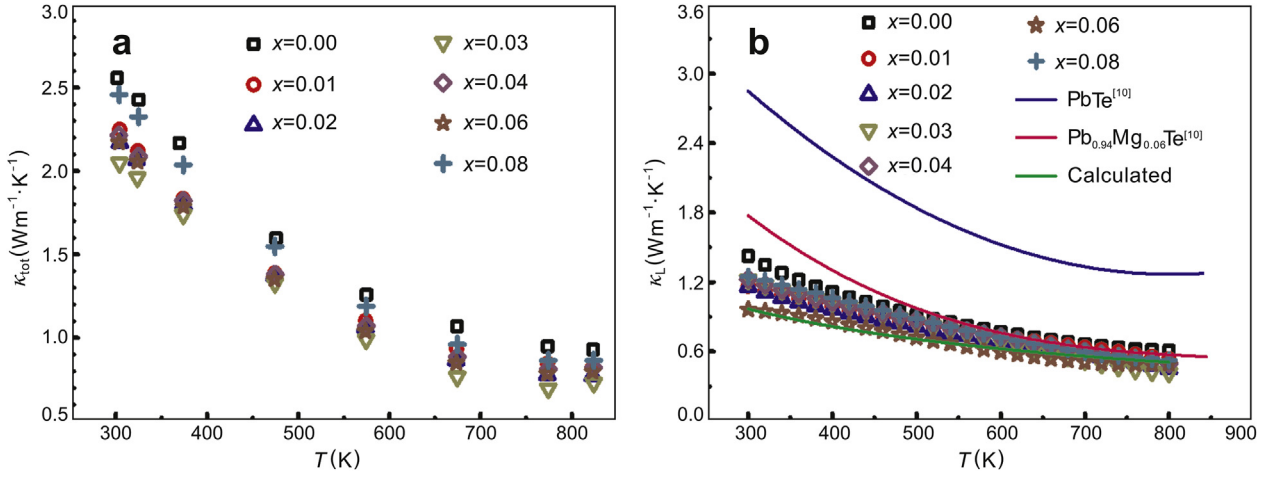

Fig. 4. Temperature dependence of (a) total and (b) lattice thermal conductivity for $Pb_{1-x}Mg_xTe_{0.8}Se_{0.2}$ samples doped with 2% Na. The blue and pink solid lines in (b) are for PbTe and $Pb_{094}Mg_{0.06}Te$ in previous work (Ref. [10]). The green line is the calculated lattice thermal conductivity for $Pb_{0.94}Mg_{0.06}Te_{0.8}Se_{0.2}$ by using the Callaway model.

further reduced to ~0.96 $Wm^{-1} K^{-1}$ for the sample $x = 0.06$. The calculated theoretical κ_L for $Pb_{0.94}Mg_{0.06}Te_{0.8}Se_{0.2}$ by the modified Callaway model is in good agreement with the experimental data. The details of the modified Callaway model can be found in previous literature [10,32].

TEM observation was carried out on the sample $Pb_{0.94}Mg_{0.06}Te_{0.8}Se_{0.2}$ ($x = 0.06$). Although all samples show no evidence of MgTe phase in the XRD patterns, Fig. 5(a) shows the typical medium magnification bright field image with platelet-like nanostructures as dark contrast embedded in the matrix, which can be seen along <100> axis group merely. The sizes of the nanostructures range from 2 to 10 nm. In Fig. 5(d) and (e), the spherical or elliptical nanostructures, general in PbTe-based TE materials, show a lower density and a smaller size than those PbTe-based materials which were reported with a good TE performance before [10,11,33]. The disarranged nanostructures will scatter the heat-carrying phonons with short and medium free mean paths (3–100 nm), resulting in a reduction in lattice thermal conductivity.

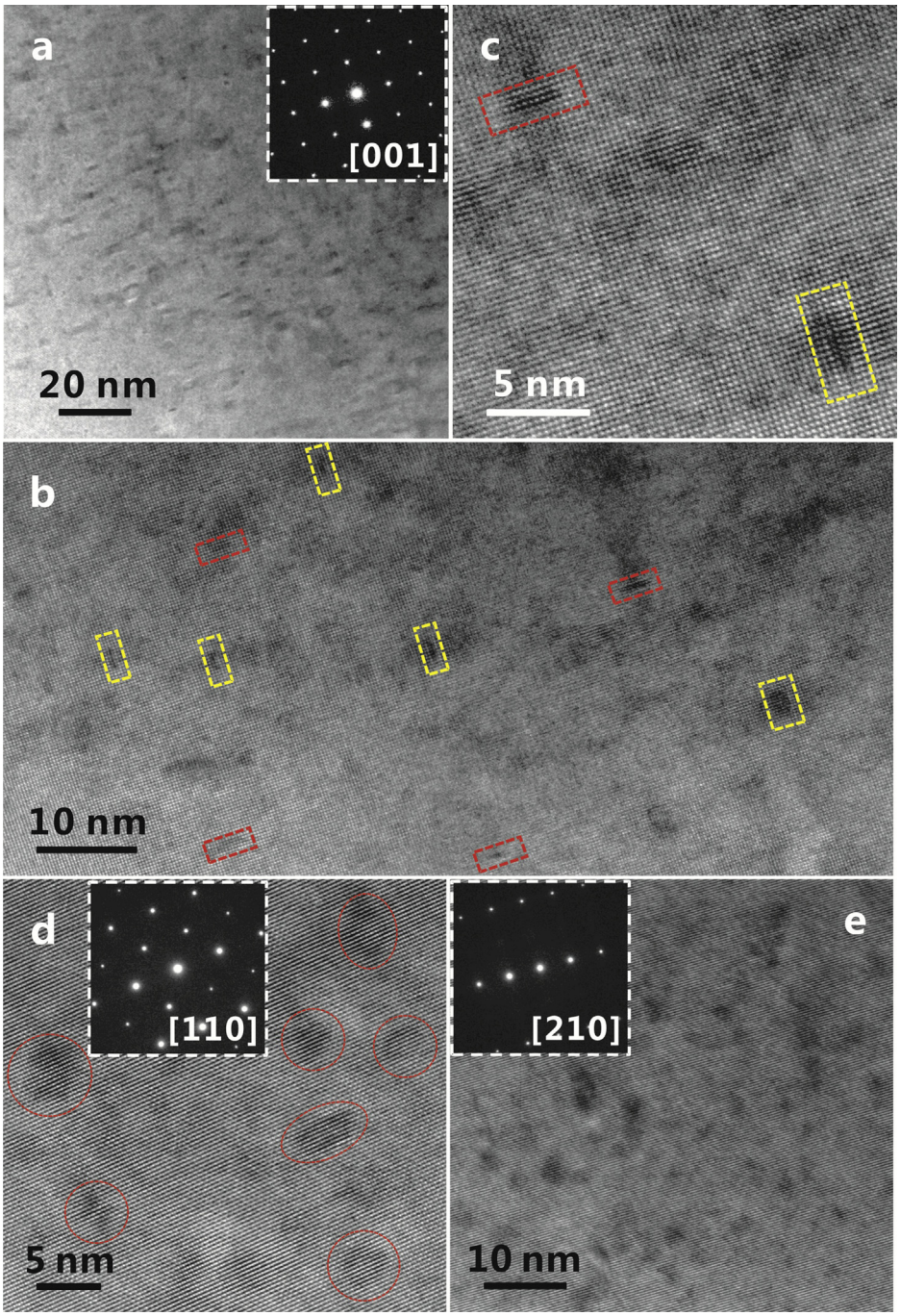

Fig. 5. TEM images of nanostructures in the sample $Pb_{0.94}Mg_{0.06}Te_{0.8}Se_{0.2}$ ($x = 0.06$) doped with 2% Na. (a) Low-magnification, (b) mid-magnification and (c) high-magnification TEM images along [001] zone axis show presence of platelet-like nanostructure. Fig. 5(d) and (e) show presence of spherical or elliptical nanostructures along [110] zone axis and [210] zone axis respectively. The electron diffraction patterns of the selected area are inserted.

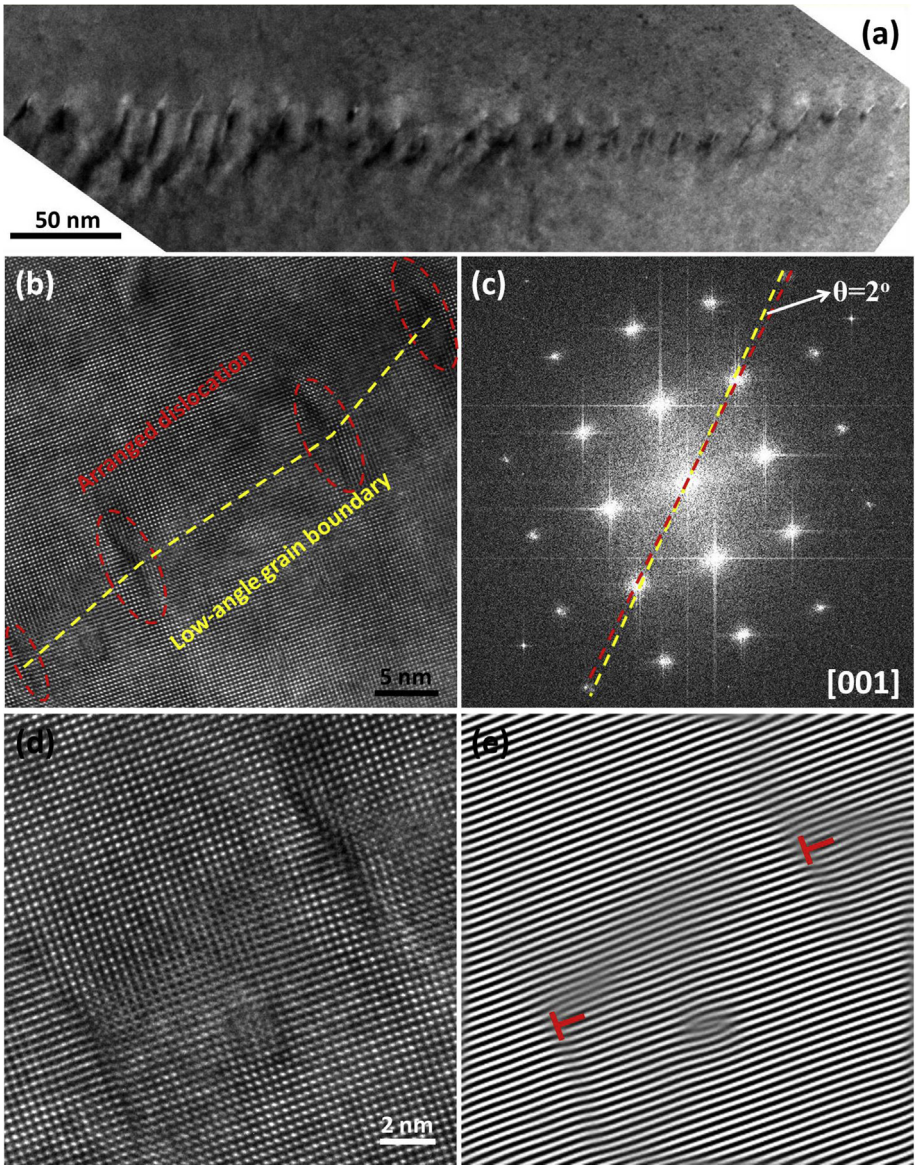

Fig. 6. TEM images of arranged dislocation at low-angle (low-energy) grain boundary in the sample $Pb_{0.94}Mg_{0.06}Te_{0.8}Se_{0.2}$ ($x = 0.06$) doped with 2% Na. Fig. 6(a) low-magnification TEM image depicts presence of densely arranged dislocation. Fig. 6(b) HRTEM image further shows that there are four dislocations at grain boundary whose FFT image is shown in Fig. 6(c). HRTEM image Fig. 6(d) and corresponding IFFT image Fig. 6(e) can also show dislocations apparently.

Fig. 6 shows the details of arranged dislocations at low-angle (low-energy) grain boundary. Densely arranged dislocations at grain boundary are displayed in Fig. 6(a) and (b), and the FFT image in Fig. 6(c) shows that these two close grains with the interfacial layer have almost the same direction with only two degrees orientation deviation. Arranged dislocation at low-angle grain boundary will scatter phonons effectively but affect electrons slightly. The misfit of the matrix and the nanostructures show the semi-coherent nature of the interface, which is also helpful in reducing the lattice thermal conductivity.

Temperature dependence of figures of merit $zT$for all samples is shown in Fig. 7 zT of ~1.8 can be obtained at 820 K for the sample $x = 0$ and its value is further improved to 2.2 by multi-alloying with Mg and Se as a result of modifying band structures and reducing the lattice thermal conductivity. Further alloying with Mg in the $PbTe_{0.8}Se_{0.2}$

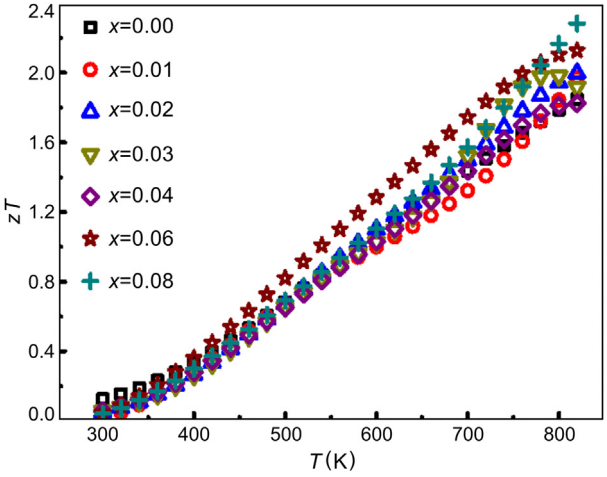

Fig. 7. Temperature dependence of zT for $Pb_{1-x}Mg_xTe_{0.8}Se_{0.2}$ doped with 2% Na samples.

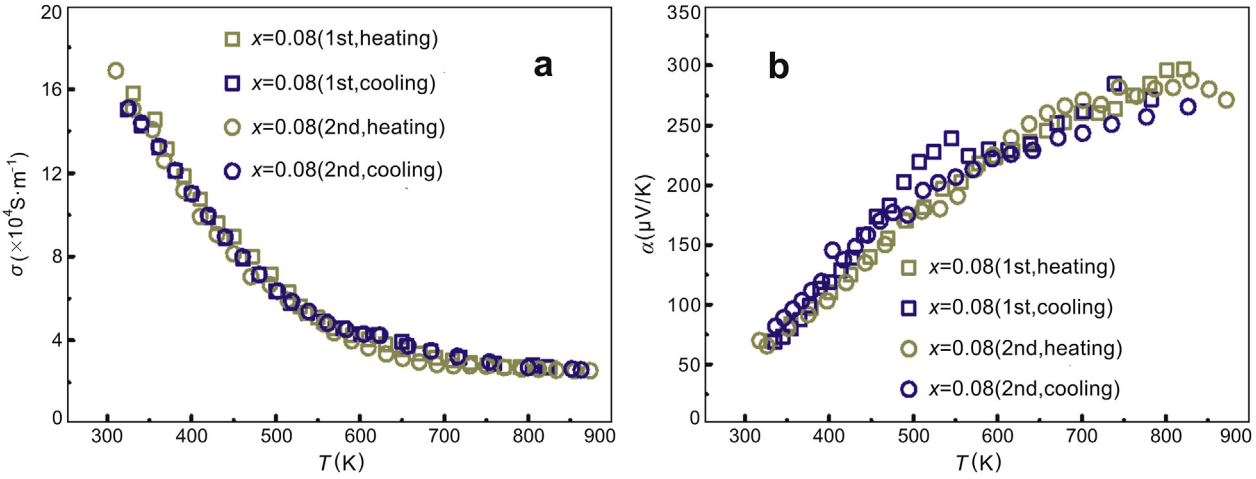

Fig. 8. Two heating–cooling cycles of (a) electrical conductivity and (b) Seebeck coefficient for the optimum composition $Pb_{1-x}Mg_xSe_{0.2}Te_{0.8}$ ($x = 0.08$).

systems widens the band gap, which effectively suppresses the bipolar diffusion at high temperatures. The nanostructures semi-coherent with the matrix also play a significant role in reducing the κ_L, synergistically resulting in a promising high zT.

Additionally, the electrical properties of the sample with optimum composition ($x = 0.08$) were tested repeatedly and the data of heating–cooling cycles are provided in Fig. 8, indicating that the material has a good thermal stability in the present conditions.

3.3. Large size bulk materials and TE performance

To develop TE devices for the large-scale commercial application, large-dimensional and homogeneous samples are needed. We fabricated a large size sample with a dimension of ~Φ42 mm × 18 mm (~200 g, relative density > 97%) as shown in Fig. 9(a). Considering that Mg is highly reactive and easy to vaporize during the melting process, synthesizing such a large dimension sample (~200 g) may bring much difficulty in preparation and cause insecurity problems. Besides, the sample with 1% MgTe also has a high peak zT of ~2.0. Thus, by comprehensively considering the TE performance and preparation feasibility and security, we fabricated the large dimension sample with the Mg content of 1% (x = 0.01). In order to check the homogeneity of the large bulk and the repeatability of the TE performance, we cut some small pellets from the large bulk to measure their properties, as shown in Fig. 9(b). Three cylinders were cut off by wire cutting, among which two cylinders are parallel to the axis (labeled as AB: Axis Boundary and AC: Axis Center), while the third one is along the radial direction (labeled as R: Radial). The cylinders were then cut into several pellets for thermal conductivity measurement. And the pellets were cut into bars for the electrical properties measurement, as shown in Fig. 9(b).

Fig. 10 shows the TE properties as a function of temperature for the samples labeled as AB-1, AB-2, AB-3 and AB-4. The electrical conductivity, the Seebeck coefficient and total thermal conductivity do not show big deviations among all samples, and even all the zT values range from ~1.8 to ~2.2. The deviation of zT is the result of comprehensive roles of various factors, including the inhomogeneous compositions and measurement uncertainties. As shown in Fig. 11, it can be concluded that relatively homogeneous distribution of high zTs can be achieved in such a large sample.

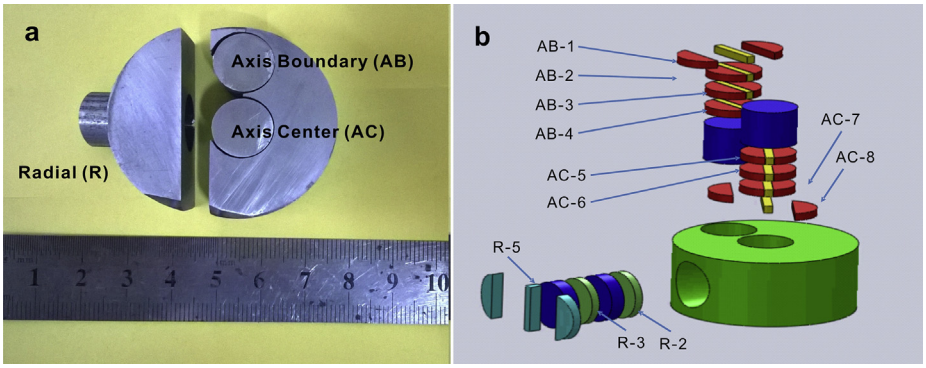

Fig. 9. (a) Pictures and (b) schematic drawing of the large size sample.

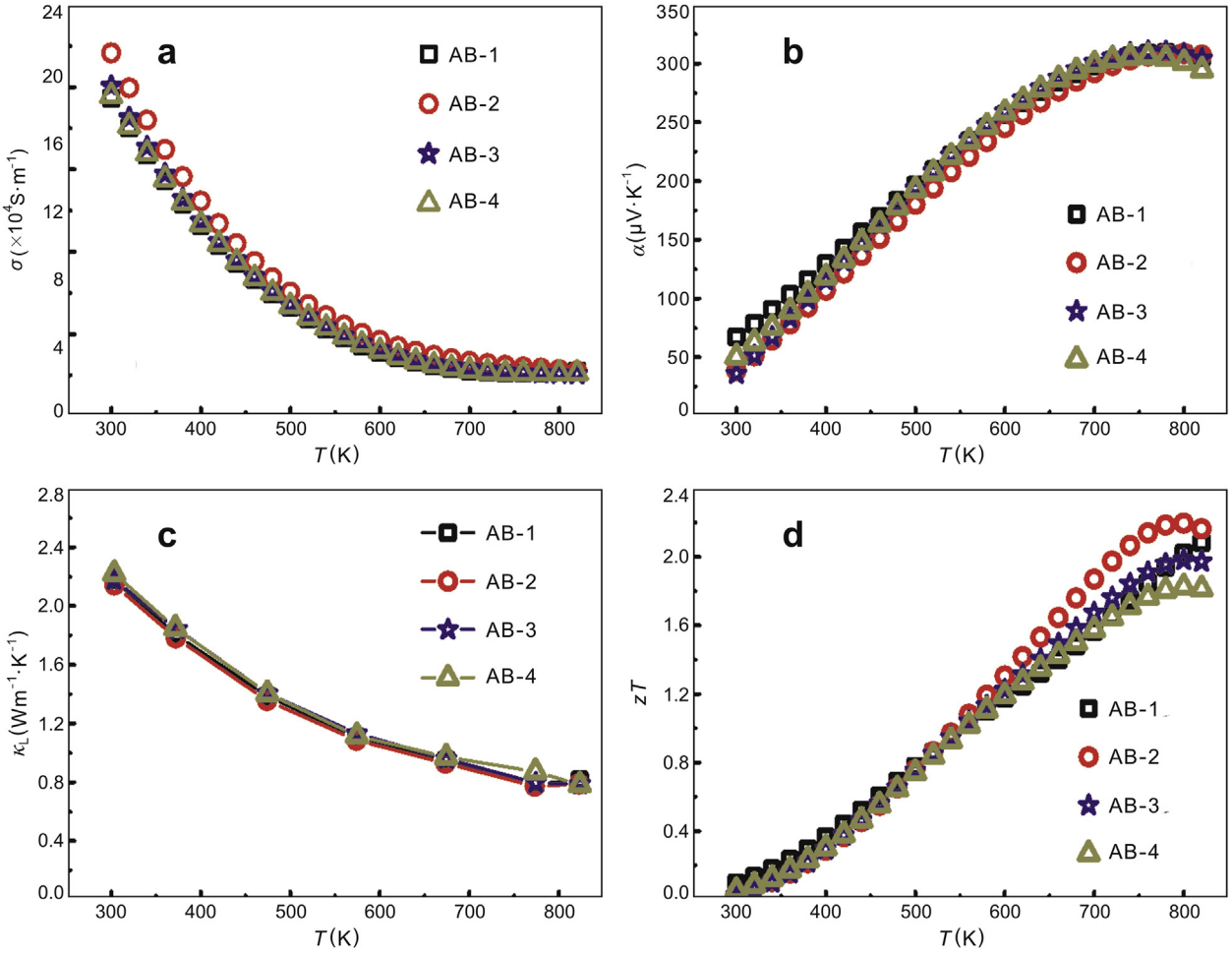

Fig. 10. Temperature dependences of (a) electrical conductivity, (b) Seebeck coefficient, (c) thermal conductivity and (d) figure of merit zT of pellets labeled as AB.

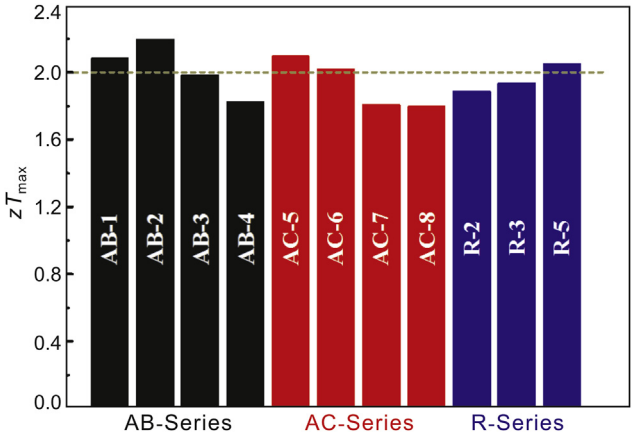

Fig. 11. Distribution of maximum of zT for all pellets cut from the large size sample.

4. Conclusions

We synthesized $Pb_{1-x}Mg_xTe_{0.8}Se_{0.2}$ solid solutions and investigated their electrical and thermal transport properties. The TE properties of $PbTe_{1-x}Se_x$ systems could be further enhanced with multi-alloying with Mg, due to the band structure optimization and reduced lattice thermal conductivity. A maximum zT of ~2.2 was reached at 820 K. The high zTs of ~1.8–2.2 were also achieved in a large size sample (~200 g), which demonstrates the realistic prospect of large-scale commercial fabrication of high performance PbTe-based TE materials.

Acknowledgment

This work was supported by the National Basic Research Program of China (2013CB632500), and the Nature Science Foundation of China (51271165 and 61534001). J.H. acknowledges the financial support from the Shenzhen Science and Technology Plan Project (No. ZDSYS20141118160434515). Transmission electron microscopy work was performed in Center of Electron Microscopy in Zhejiang University, Hangzhou, China (H.J.W).

References

[1] Goldsmid HJ. Introduction to thermoelectricity. Springer; 2009.
[2] Snyder GJ, Toberer ES. Complex thermoelectric materials. Nat Mater 2008;7:105–14.
[3] Zhang X, Zhao LD. Thermoelectric materials: energy conversion between heat and electricity. J Materiomics 2015;1:92–105.

[4] Ioffe AF. Semiconductor thermoelements and thermoelectric cooling. London: Infosearch; 1957.
[5] Pei YZ, Shi XY, LaLonde A, Wang H, Chen LD, Snyder GJ. Convergence of electronic bands for high performance bulk thermoelectrics. Nature 2011;473:66–9.
[6] Li W, Chen ZW, Lin SQ, Chang YJ, Ge BH, Chen Y, et al. Band and scattering tuning for high performance thermoelectric $Sn_{1-x}Mn_xTe$alloys. J Materiomics 2015;1:307–15.
[7] Heremans JP, Wiendlocha B, Chamoire AM. Resonant levels in bulk thermoelectric semiconductors. Energy EnvironmSci 2012;5:5510–30.
[8] Jaworski CM, Wiendlocha B, Jovovic V, Heremans JP. Combining alloy scattering of phonons and resonant electronic levels to reach a high thermoelectric figure of merit in PbTeSe and PbTeS alloys. Energy EnvironmSci 2011;4:4155–62.
[9] Fu CG, Zhu TJ, Liu YT, Xie HH, Zhao XB. Band engineering of high performance p-type FeNbSb based half-Heusler thermoelectric materials for figure of merit $zT > 1$. Energy EnvironmSci 2015;8:216–20.
[10] Zhao LD, Wu HJ, Hao SQ, Wu CI, Zhou XY, Biswas K, et al. All-scale hierarchical thermoelectrics: MgTe in PbTe facilitates valence band convergence and suppresses bipolar thermal transport for high performance. Energy Environm Sci 2013;6:3346–55.
[11] Biswas K, He JQ, Blum ID, Wu CI, Hogan TP, Seidman DN, et al. High-performance bulk thermoelectrics with all-scale hierarchical architectures. Nature 2012;489:414–8.
[12] Pei YZ, Heinz NA, LaLonde AD, Snyder GJ. Combination of large nanostructures and complex band structure for high performance thermoelectric lead telluride. Energy EnvironmSci 2011;4:3640–5.
[13] Wang HC, Bahk JH, Kang C, Hwang J, Kim K, Kim J, et al. Right sizes of nano-and microstructures for high-performance and rigid bulk thermoelectrics. Proc Natl Acad Sci 2014;111:10949–54.
[14] Ravich YI, Efimova BA, Smirnov IA. Semiconducting lead chalcogenides. Plenum Publishing Corporation; 1970.
[15] Rowe DM. Thermoelectrics handbook: macro to nano. CRC Press; 2005.
[16] Liu XH, Zhu TJ, Wang H, Hu LP, Xie HH, Jiang GY, et al. Low electron scattering potentials in high performance $Mg_2Si_{0.45}Sn_{0.55}$ based thermoelectric solid solutions with band convergence. Adv Energy Mater 2013;3:1238–44.
[17] Liu W, Tang XF, Li H, Yin K, Sharp J, Zhou XY, et al. Enhanced thermoelectric properties of n-type $Mg_{2.16}(Si_{0.4}Sn_{0.6})_{1-y}Sb_y$ due to nano-sized Sn-rich precipitates and an optimized electron concentration. J Mater Chem 2012;22:13653–61.
[18] Tan GJ, Shi FY, Hao SQ, Chi H, Bailey TP, Zhao LD, et al. Valence band modification and high thermoelectric performance in SnTe heavily alloyed with MnTe. J Am Chem Soc 2015;137:11507–16.
[19] Wu HJ, Chang C, Feng D, Xiao Y, Zhang X, Pei YL, et al. Synergistically optimized electrical and thermal transport properties of SnTe via alloying high-solubility MnTe. Energy & Environ Sci 2015;8:3298–312.
[20] Jaworski CM, Nielsen MD, Wang H, Girard SN, Cai W, Porter WD, et al. Valence-band structure of highly efficient p-type thermoelectric PbTe-PbS alloys. Phys Rev B 2013;87:045203.
[21] Korkosz RJ, Chasapis TC, Lo SH, Doak JW, Kim YJ, Wu CI, et al. High ZT in p-type $(PbTe)_{1-2x}(PbSe)_x(PbS)_x$ thermoelectric materials. J Am Chem Soc 2014;136:3225–37.
[22] Pei YZ, LaLonde AD, Heinz NA, Shi XY, Iwanaga S, Wang H, et al. Stabilizing the optimal carrier concentration for high thermoelectric efficiency. Adv Mater 2011;23:5674–8.
[23] Wang H, Pei Y, LaLonde AD, Synder GJ. Heavily doped p-type PbSe with high thermoelectric performance: an alternative for PbTe. Adv Mater 2011;23:1366–70.
[24] Blachnik R, Igel R. Thermodynamic properties of IV–VI-compounds: leadchalcogenides. Z Naturforsch B 1974;29:625–9.
[25] Yang SH, Zhu TJ, Sun T, He J, Zhang SN, Zhao XB. Nanostructures in high-performance $(GeTe)_x(AgSbTe_2)_{100-x}$ thermoelectric materials. Nanotechnology 2008;19:245707.
[26] Pei YZ, LaLonde AD, Iwanaga S, Snyder GJ. High thermoelectric figure of merit in heavy hole dominated PbTe. Energy EnvironmSci 2011;4:2085–9.
[27] Pei YZ, May AF, Snyder GJ. Self-Tuning the carrier concentration of $PbTe/Ag_2Te$ composites with excess Ag for high thermoelectric performance. Adv Energy Mater 2011;1:291–6.
[28] Pei YZ, LaLonde AD, Wang H, Snyder GJ. Low effective mass leading to high thermoelectric performance. Energy EnvironmSci 2012;5:7963.
[29] Litz MT, Watanabe K, Korn M, Ress H, Lunz U, Ossau W, et al. Epitaxy of $Zn_{1-x}Mg_xSe_yTe_{1-y}$on (100)InAs. J Cryst Growth 1996;159:54–7.
[30] Crocker AJ, Sealy BJ. Some physical properties of PbTe-MgTe alloy system. J PhyChem Solids 1972;33:2183–90.
[31] Smirnov IA, Vinogradova MN, Kolomoets NV, Sysoeva L. Thermal conductivity of heavily doped p-type PbTe. SovPhysSolid State 1968;9:2074–9.
[32] Callaway J. Model for lattice thermal conductivity at low temperatures. Phys Rev 1959;113:1046–51.
[33] Wang HZ, Zhang QY, Yu B, Wang H, Liu WS. Transmission electron microscopy study of Pb-depleted disks in PbTe-based alloys. J Mater Res 2011;26:912–6.

Tiezheng Fu is a Ph.D. candidate in Materials Science at Zhejiang University, China. His research focuses on IV–VI thermoelectric compounds under the supervision of Prof. Xinbing Zhao and Prof. Tiejun Zhu. He was awarded Bachelor of Engineering Degree in Materials Science and Engineering from Zhejiang University, China, in 2014.